Martinez-Vazquez, P., Gkantou, M. and Baniotopoulos, C. (2018) Strength and ductility demands on wind turbine towers due to earthquake and wind load. Proceedings of the Institution of Civil Engineers–Structures and Buildings. https://doi.org/10.1680/jstbu.17.00154

# Strength and ductility demands on wind turbine towers due to earthquake and wind load

P. Martinez-Vazquez, M. Gkantou, C. Baniotopoulos

*School of Engineering, Civil Engineering Department, The University of Birmingham, Edgbaston B15 2TT, Birmingham, United Kingdom*

## Abstract

In earthquake prone areas, wind and earthquake loads are assumed to be statistically uncorrelated, therefore their interaction is ignored by existing design guidelines. However, the fact that strong earthquake events are commonly followed by aftershocks and that wind is constantly flowing at high speeds around wind farms increase the probability of their joint occurrence, thus making current design assumptions questionable. This investigation shows that multi-hazard scenarios magnify strength demands of wind turbine towers designed against isolated load conditions, hence modifying their performance level. It is also shown that, under certain conditions, the probabilities associated to the joint occurrence of earthquake and low to strong wind events match or exceed those related to the original design, thus rendering wind energy infrastructure susceptible to unforeseen damage.

Key words: Earthquake; Wind; Load Interaction; Multi-hazard; Performance level; Wind turbine tower

## Notation

| | |
|---|---|
| $A$ | Area exposed to wind |
| $C_D$ | Drag coefficient |
| $C_{prob}$ | Probability factor |
| $D$ | Section diameter |
| $F$ | Force |
| $H$ | Height of building |
| $I_u$ | Turbulent intensity |
| $M_s$ | Magnitude scale |
| $N$ | Number of earthquake events |
| $P_J$ | Probability associated to load J |
| $PGA$ | Peak ground acceleration |
| $R_\mu$ | Strength reduction factor |
| $\bar{U}$ | Average wind velocity |
| $V_{s30}$ | Upper 30-m mean shear wave velocity |
| $a$, $b$ | Site-dependent parameters |
| $d$ | Structural displacement |
| $m$ | Structural mass |
| $n_0$ | Fundamental frequency of vibration |
| $p$ | Load |
| $s$ | Load gradient |
| $t$ | Section thickness |
| $u_y$ | Yield displacement |
| $z$ | Vertical coordinate |
| $\Gamma$ | Characteristic structural density |
| $\beta$ | Modal exponential |
| $\Upsilon$ | Generalised quantity |
| $\varphi$ | Modal shape |
| $\mu$ | Ductility factor |
| $\rho$ | Air density |
| $\sigma$ | Standard deviation of wind velocity |
| $\omega$ | Natural frequency |
| $\xi$ | Structural damping |

## 1. Introduction

In the past decades, regions across the world have been identified where the energy production of Class I and Class II wind energy increases exponentially. This is largely due to the availability of natural resources, technological developments and qualified labour. The fast growth of energy generation however requires careful consideration of the type of infrastructure that can fulfil the demands in terms of strength, resilience and innovation. In earthquake-prone regions, tectonic and environmental conditions make infrastructure often susceptible to earthquakes and wind effects both during construction and once in operation. Notwithstanding that, current engineering practice disregards their simultaneous occurrence even though past earthquake records show that further ground accelerations can occur within days or even hours from main events. Examples of this include the earthquake that hit the Sichuan Province in China in 2008 (Ms = 7.9) which was followed by 12 weeks with 42 aftershocks ranging in magnitude between $5 < Ms < 6.4$, killing over 87,000 and leaving over £56bn in losses (Daniell et al., 2012). The Great East Japan Earthquake felt in 2011 (Ms = 9.0), killing more than 15,000, was followed by 408 aftershocks ($Ms \geq 5.0$) within 96 hr, 68 of those of $Ms \geq 6.0$ and 5 of $Ms \geq 7.0$ (Matsutani, 2011). More recently, the earthquakes that hit Ecuador in 2016 (Ms = 7.8) killing over 600, were followed by over 55 aftershocks in the first 24 hours (Shankar, 2016).

Past research has contributed to better understand the mechanisms through which extreme load events affect infrastructure. Martinez-Vazquez (2017) showed that the combination of earthquakes and wind would decrease the value of strength reduction factors that are calculated by ignoring the impact of wind during an earthquake. Kiyomiya et al. (2002) suggested that wind turbines have adequate earthquake resistance provided these are designed against typhoons, which could be the case of offshore wind turbines but is not shared practice for onshore infrastructure design. Furthermore, Diaz and Suarez (2014) demonstrated that an operational earthquake combined with design wind load tend to over-stress the tower section hence increasing the strength demand established under isolated wind conditions. The present paper thus aims at enhancing our understanding of multi-hazard load conditions and their effect on wind energy infrastructure.

The paper is organised as follows, Section 2 describes the assembling process of two databases, one containing historical earthquake records and the other containing simulated wind fields. Section 3 focuses on the estimation of generalised forces acting on three wind turbine towers and the calculation of their dynamic response. The associated probabilities are discussed in Section 4 whilst the estimation of strength and ductility demands related to multi-hazard scenarios is presented in Section 5. Some final remarks are provided in Section 6.

## 2. Earthquake and wind record database

Earthquake records of magnitude $5.3 \leq Ms \leq 7.36$ recorded on alluvium and with distances from geological faults of up to 57 km were downloaded from the PEER (2016) ground motion database. These records are assumed to be representative of alluvium and firm soils. It has been shown in Miranda (1993) that without much variation they would produce similar strength demands to structures located on either soil type. These records have a duration which oscillates between 30 and 80 s and were measured at a time interval of 0.1 s. The list of historic earthquake records is provided in Table 1 which also shows the associated epicentral distance, shear wave velocity ($vs_{30}$), and peak ground acceleration (PGA).

**TABLE 1**

On the other hand, a wind record database was established based on the simulation procedure reported in Martinez-Vazquez and Rodriguez-Cuevas (2007) which follows the conditional simulation proposed by Vanmarcke et al. (1993). The simulation algorithm requires knowledge of recorded data in at least two points within the region of interest and enables inferring properly correlated wind data series at intermediate points. The two initial data series were calculated by using classical Monte Carlo techniques whereas intermediate points were calculated at 11 stations covering 250 m along a vertical axis. The mean velocity $\overline{U}$ and turbulence intensity $I$ - defined as the ratio between the standard deviation and the mean ($\sigma/\overline{U}$) - are shown for each simulation point in Table 2 for the case in which $\overline{U}$ =20 ms$^{-1}$. This table also shows how simulated *(s)* and theoretical *(t)* values compare.

**TABLE 2**

According to the data in Table 2, the average ratio $\overline{U}_t/\overline{U}_s$ is 1.028 whereas the mean square error associated to the simulated turbulence intensity is 0.002. The theoretical wind velocity and turbulence intensity were determined based on a standard exponential law i.e. $U_z = (z/z_{ref})^{\alpha}$ using $\alpha$ = 0.22 and $I_{u,10}$ = 0.295 which corresponds to suburbs. Table 3 shows the target and calculated cross-correlation in the lower and upper triangular matrices respectively, where Point 1 corresponds to that located at $z$ = 10 m. It can be seen in the table that the accuracy of the simulation increases with the proximity between points – see for example the values around the main diagonal. The overall mean square error across cross-correlation results is 0.0073 which was considered acceptable for this investigation.

**TABLE 3**

### 3. Generalised forces acting on wind turbines and related dynamic effects

Three wind turbine towers of 150 m, 200 m and 250 m height were identified. These are assumed to be made of steel with specific weight of 7850 kgm$^{-3}$, Young's modulus of 200×10$^9$ Nm$^{-2}$, damping level of 5%, and having variable section across their length whilst fixed at their base. The geometry and natural vibration frequency of each tower are shown in Table 4.

**TABLE 4**

Earthquake forces *($F_{EQ}$)* are proportional to the mass of the structure whilst wind forces *($F_W$)* were derived from Bernoulli's principle: $F_W = 1/2\ \rho\ C_D A\ \overline{U}^2$ – where ρ is the density of the air, $C_D$ is a drag coefficient (taken as 1.4), and $A$ is the projected area of the segment exposed to wind. Generalised forces, $F_{EQ}^*$ and $F_W^*$, were calculated by using Eq. (1), where $\Upsilon(z)$ represents force or structural mass per unit length, z is a vertical coordinate, $\lambda$ equals 1 and 2 for $F^*$ and $M^*$ respectively, $\phi$ is the fundamental modal shape which was approximated by $\phi(z) = (z/H)^{\beta}$ – with $\beta$ = 1.5 whilst taking $H$ as the height of the tower.

$$\Upsilon^* = \int_0^H \phi(z)^{\lambda} \Upsilon(z) dz \qquad (1)$$

Generalised forces were combined to find the total amount acting on the wind turbines. This is shown in Table 5 for seven levels of wind, including the case in which $\overline{U}$ equals zero. This table also shows the average estimated ratio $F_{EQ}^*/F_W^*$. Earthquake loading dominates for low values of wind velocity, however this condition changes rapidly as the value of $\overline{U}$ increases. For example when $\overline{U}$ = 5 ms$^{-1}$ earthquake are about twice wind forces whilst when $\overline{U}$ = 10 ms$^{-1}$ earthquake are about half wind forces. At the point of the design wind speed, earthquake forces are about 12% of wind peak forces.

**TABLE 5**

Total generalised forces reported in Table 5 were used to determine the dynamic response of the wind turbines listed in Table 4, assuming linear-elastic performance. This was done through the numerical integration of Eq. (2) whose solution is given by Eq. (3).

$$m\ddot{d} + c\dot{d} + kd = p(t) \tag{2}$$

$$d(t) = e^{-\xi\omega\Delta t}\left[\left(d(0) - \frac{p_i}{k} + \frac{2s\xi}{\omega_n k}\right)\cos(\omega_D \Delta t) + \left(\dot{d}(0) + d(0)\xi\omega_n - \frac{p_i\xi\omega_n}{k} + \frac{2s\xi^2}{k} - \frac{s}{k}\right)\frac{sin(\omega_D\Delta t)}{\omega_D}\right]\frac{p_i}{k} + \frac{s\Delta t}{k} - \frac{2s\xi}{\omega_n k} \tag{3}$$

In Eq. (2) and (3) *m*, *c*, and *k* represent the system's mass, damping coefficient, and stiffness; *d(t)* and $\dot{d}(t)$ are displacement and velocity of response respectively; *p(t)* is the time-varying force; $p_i$ and *s* represent the *i-th* force and its gradient, in the context of the numerical integration; $\omega_n$ and $\omega_D$ are the undamped and damped frequency whilst $\xi$ represents the fraction of critical damping. The results of the numerical integration are shown in Table 6.

**TABLE 6**

The results in Table 6 show a considerable increase of peak displacements for relatively low levels of wind acting on assumed earthquake-resisting structures. For example, when $\overline{U} = 2.5$ ms$^{-1}$ the estimated increase is of 21%, 35%, and 38% on the towers of 150 m, 200 m, and 250 m tall, respectively, whereas when $\overline{U}$ = 5 ms$^{-1}$ those figures become 114%, 170%, and 219%. This suggests that the combined effect of earthquake and wind load can be significantly higher than those due to earthquakes only, even for relatively low levels of wind. However, infrastructure could also be designed to withstand wind load only in which case the earthquake load would have a different level of impact depending on the design wind load. Wind-resisting design is examined in more detail in the following sections.

## 4. Probabilities associated to wind and earthquake events

Eurocode 1 (European Standard, 2010) associates wind design loads to a 50-year return period whose probability of annual exceedance is $P_{50}$ = 0.02. The norm also provides Eq. (4) to scale the 10-min design wind velocity, $\overline{U}_{50}$ for other probability levels.

$$C_{prob} = \left[\frac{1 - K \cdot ln\big(-ln(1-p)\big)}{1 - K \cdot ln\big(-ln(0.98)\big)}\right]^n \tag{4}$$

In Eq. (4) *K* is a shape parameter that depends on the coefficient of variation of the extreme-value distribution, *n* is a constant number, $C_{prob}$ is the probability factor and *p* represents probability. Eurocode 1 recommends *K* = 0.2 and *n* = 0.5.

$$log_{10}N = a - bM \tag{5}$$

On the other hand, the Gutenberg-Richter law quoted in Eq. (5), establishes a relationship between frequency of earthquake events and their magnitude. In this equation, *N* represents the number of events happening within a year, having magnitude $\geq M$ and *a, b* are site-dependent constants. It follows that Eq. (4) and (5) can be used to infer the magnitude of earthquake events associated to probability values ($P_{EQ}$) which, paired with those related to wind ($P_W$), match the standard probability of wind-resisting design i.e. $P_{EQ} \cdot P_W$ = 0.02. This is shown in Table 7 for a set of randomly selected locations across the world, assuming $\overline{U}_{50} = 20$ ms$^{-1}$.

**TABLE 7**

In Table 7, rows 3 and 1 relate to local average wind speeds and their probability of occurrence as per Eq. (4). Row 4 provides the probability associated to seismic magnitude depending on location. There are five countries listed in Table 7 with their respective value of $M_s$ which directly links to their probability of occurrence as per Eq. (5). The reason those specific probabilities - quoted in rows 1 and 4 of the Table, have been selected is because their product matches the probability associated to the design wind speed, which according to Eurocode 1 (European Standard, 2010), corresponds to the design wind speed here assumed to be of 20 ms$^{-1}$. Hence these are meaningful combinations derived from the simultaneous occurrence of earthquake and wind events. According to the data shown in Table 7, $\overline{U} = 10.33$ ms$^{-1}$ would always be exceeded in a year – see rows 1 and 3, whilst $\overline{U} = 18.92$ ms$^{-1}$ and 18.05 ms$^{-1}$ considerably exceed the probability of the design wind speed as reported in row 1.

The joint occurrence of earthquake and wind events listed on each column of Table 7 therefore match the single probability associated to the design wind load, and define a sub-set of multi-hazard scenarios that tend to magnify the strength and ductility demand of wind turbine towers, as discussed in the following section.

## 5. Strength and ductility demands associated to earthquake and wind load

The relationship between strength and ductility determine the performance level of structures. Although such parameterisation is more common in earthquake than wind applications, both earthquake and wind effects can be merged to quantify linear-elastic and plastic structural performance through strength reduction factors, as in Martinez-Vazquez (2017). In the present investigation the strength demands imposed by multi-hazard conditions was quantified in simple terms through the second moment of area that is required to ensure fully-operational conditions of wind energy infrastructure. On a second stage, a map was established between the estimated demands of strength and the corresponding ductility level. This enabled to assess the performance level of the wind turbine towers subject to earthquake and wind joint effects.

### *5.1 Strength Demand*

The relationship $F_{EQ}{}^{*}/\,F_{W}{}^{*}$ provided in Table 5 was taken to find the required section of prismatic steel towers so that the ratio between the maximum displacement and the displacement that induces the yield stress on the base material, match. To that end, wind and earthquake forces were estimated with Eq. (6).

$$F_W^* = \frac{F_{EQ}^* + F_W^*}{F_{EQ}^*/F_W^* + 1} \tag{6a}$$

$$F_{EQ}^* = \frac{F_{EQ}^* + F_W^*}{F_W^*/F_{EQ}^* + 1} \tag{6b}$$

Strength demands across the three wind turbine towers were defined in terms of the ratio $I_{EQ+W}/I_{EQ\ or\ W}$, where $I_J$ is the second moment of area associated to material yielding, given the load $j$. The strength demand associated to design earthquake ($I_{EQ}$) or wind load ($I_W$) is thus magnified when this relationship exceeds 1. Results of this analysis are shown in Table 8 considering two load scenarios: average values associated all 40 earthquake records listed in Table 1 (EQ#1-40), and values characterising isolated events, namely, EQ#5, EQ#24, and EQ#38. All these combinations being consistent with the probability analysis reflected in Table 7. For example, EQ#5 which has a magnitude $M_s$ = 5.3, would be exceeded every year in earthquake prone areas (Global Data) as it is lower than $M_s$

= 6.36, therefore it can be combined with any wind event. EQ#24 with $M_s$ = 6.53 can be combined with wind events having $\overline{U} \leq 18.92$ ms$^{-1}$ whereas EQ#38 with $M_s$ = 7.01 can be combined with wind events having $\overline{U} \leq 18.05$ ms$^{-1}$. It is also worth noting that values in Table 8 which are higher than 1 indicate that the multi-hazard condition would exceed the design strength, $I_{EQ\ or\ W}$.

**TABLE 8**

From Table 8 it becomes apparent that wind turbine towers would primarily be designed to withstand wind load since all values of $I_{EQ+W}/I_{EQ}$ are above 1 whilst most values of $I_{EQ+W}/I_W$ are below 1. The sub-set 18.05 ms$^{-1}$ $\leq \overline{U} \leq$ 20 ms$^{-1}$ however defines a region of magnified strength demands ranging between $1 \leq I_{EQ+W}/I_W \leq 1.206$. Note that EQ#24 in Table 8 could not be combined with $\overline{U}$ = 20 ms$^{-1}$ because its magnitude exceeds $M_s$ = 6.36 therefore the combined probability of those events exceeds $P_{50}$ = 0.02. With the same criteria two other combinations of EQ#38 were discarded. Keeping with wind resisting design, the combined action of $\overline{U} = 18.92$ ms$^{-1}$ and the average of the set EQ#1-40 would match the strength demand imposed by the design wind load, whereas the demand of strength would be exceeded in 20.6% if the same wind speed did occur simultaneously with an earthquake of $M_s$ = 6.53 (e.g. EQ#24). The latter identifies the worst case scenario as derived from this investigation.

*5.2 Ductility Demand*

In Martinez-Vazquez (2017), a relationship between strength reduction factors ($R_\mu$) associated to multi-load scenarios and structural ductility ($\mu$) is established. The definition of these parameters is given in Eq. (7) and (8) – where $F$ is the restoring force required to keep inelastic displacements within the limit of the ductility factor $\mu$ and $u_y$ is the displacement that limits linear elastic structural performance.

$$R_\mu = \frac{F(\mu=1)}{F(\mu=\mu)} \tag{7}$$

$$\mu = {u_{max}}/{u_y} \tag{8}$$

In that study $\Gamma = \frac{M^*}{\sqrt{H^2+W^2+L^2}}$ is defined to characterise the density of structures - where $M^*$ is the generalised mass and *H-W-L* are side dimensions of prismatic buildings. The relevant strength reduction factors (SRFs) presented in Martinez-Vazquez (2017) are reproduced here in Fig. 1 and Fig. 2, for cases where $\overline{U} = 15$ and 20 ms$^{-1}$ and when $\Gamma$ takes values of 1.91, 60.43, and 17.78.

**FIGURE 1**
**FIGURE 2**

For circular shapes, let $\Gamma = \frac{M^*}{\sqrt{H^2+D^2}}$ - where $D$ represents the diameter of the steel towers. This results in $\Gamma$ = 2.33 Ton/m, 2.94 Ton/m, and 4.17 Ton/m, for wind turbine towers of 150 m, 200 m, and 250 m height, respectively. It follows that the magnification of strength demands highlighted in Table 8 can be expressed in terms of ductility demand, as suggested by Eq. (7) and (8). By interpolation of the curves shown in Fig. 1 and 2, the average ductility demands estimated across the three wind turbine towers can be established. This is shown in Table 9.

**TABLE 9**

The results shown in Table 9 show that the combined action of wind and earthquakes can trigger inelastic performance of wind turbine towers i.e. $\mu > 1$. It is also seen that both strength and ductility

demands equal 1 when $\overline{U} = 18.92$ ms$^{-1}$ and considering all earthquake records in the database - noting that this wind speed is lower than the assumed design wind speed $\overline{U}_{50} = 20$ ms$^{-1}$. Furthermore, when the expected earthquake event i.e. EQ#1-40 occurs simultaneous to $\overline{U}_{50}$ the strength and ductility demand both exceed a design limited by the yield condition in 12% and 37% respectively. If particular events such as EQ#5, EQ#24, and EQ#38 are considered, strength demand exceedances oscillate between 3.2% and 20.6% whilst the associated ductility demands would surpass the yield condition in amounts ranging from 9% to 62%.

## 6. Final Remarks

This research identifies a narrow yet existing probability that earthquake and wind effects modify the performance level of wind energy infrastructure. The estimated strength and ductility demand of wind turbine towers indicate that under certain conditions these can undergo unforeseen inelastic performance during extreme events. This is not addressed by current engineering practice which is based on the assumption that multi-hazard scenarios are extremely rare and that no relationship can be established between earthquake and wind events. The evidence however demonstrates that the frequency of occurrence of earthquakes of medium to high intensity is not rare. According to NOAA (2017) a total of 1142 earthquakes of $5.3 \leq \text{Ms} \leq 7.01$ occurred across the world in the last 50 years (1966-2016) with as many as 173 recorded in the last 5 years (2011-2016) and 28 of those in 2016. The situation depicted in this investigation could be worse if we consider earthquake events of higher magnitude. NOAA (2017) reports a total of 418 ground motions of $7.01 \leq \text{Ms} \leq 9.9$ in the last 50 years whilst 62 and 11 of those events were seen in the period 2011-2016 and during 2016, respectively. The recent events recorded in Mexico included two major earthquakes within a period of two weeks in September 2017 (CNN, 2017) with one of them nearly clashing with hurricane Katia on 8 September 2017 (ABC News, 2017). This adds further arguments against current design assumptions which ignore multi-hazard scenarios. It seems therefore necessary to consider regional risk to extreme events in the formulation of a more robust design framework for practical use.

## References


ABC News, 2017. Hurricane Katia mudslide leaves two dead in Mexico after earthquake clean-up begins. Available at www.abc.net.au/news/2017-09-10/deadly-quake-hurricane-katia-a-one-two-punch-for-mexico/8889064 [Accessed on 20.09.17]

Bayrak Y, Öztürk S, Koravos G C, Leventakis GA and Tspanos TM (2008) Seismicity assessment for the different regions in and around Turkey based on instrumental data: Gumbel first asymptotic distribution and Gutenberg-Richter cumulative frequency law. Natural Hazards and Earth Sciences 8(1): 109-122

CNN, 2017. Mexico had two major earthquakes this month. Here's why. Available at http://edition.cnn.com/2017/09/20/americas/mexico-two-earthquakes-in-one-month/index.html [Accessed on 20.09.17]

Daniell JE, Vervaeck A, Khazai B and Wenzel F (2012) Worldwide CATDAT Damaging Earthquakes Database in conjunction with Earthquake-report.com - Presenting Past and Present Socio-Economic Earthquake Data. Proceedings of the 15th Conference on Earthquake Engineering 15WCEE, Lisbon, Portugal, 24-28 September

Díaz O and Suárez LE (2014) Seismic analysis of wind turbines. Earthquake Spectra 30(2): 743-765

European Standard (2010) Eurocode 1: Actions on structures – Part 1-4: General actions – Wind actions. European Committee for Standardization, Brussels.

Kiyomiya O, Rikiyi T and Van Gelder HAJM (2002) Dynamic response analysis of onshore wind energy power units during earthquakes and wind. Twelfth International Offshore and Polar Engineering Conference. Kitakyushu, Japan, May 26-31

Pacific Earthquake Engineering Research Centre (PEER) (2016) PEER ground motion database http://ngawest2.berkeley.edu/#disclaimer [accessed on 19.03.2016]

Martinez-Vazquez P (2017) Strength reduction factors for the combined action of wind and earthquakes. Structures and Buildings. DOI: dx.doi.org/10.1680/jstbu.16.00086.

Martinez-Vazquez P and Rodriguez-Cuevas N (2007) Wind field reproduction using neural networks and conditional simulation. Engineering Structures 29: 1442-1449

Matsutani M (2011) Why so many aftershocks? Why so large? The Japan Times. Available at https://www.japantimes.co.jp/news/2011/04/14/national/why-so-many-aftershocks-why-so-large/#.WtslWcgvzD4 [Accessed on 21.04.2018]

Miranda E (1993) Site-dependent strength reduction factors. Journal of Structural Engineering ASCE, 119(5): 1319-1338

NERC (2017) Seismicity and earthquake Hazard in the UK. British Geological Survey. Environmental Science Centre Keyworth, Nottingham, United Kingdom

NOAA (2017) Earthquake data and information. National Centers for Environmental Information – National Oceanic and Athmospheric Administration. Available at https://www.ngdc.noaa.gov/hazard/earthqk.shtml [30.04.17]

Papazachos, BC, Kiratzi AA and Karacostas BG (1997) Toward a homogeneous moment-magnitude determination for earthquakes in Greece and the surrounding area. Bulletin of the Seismological Society of America 87(2): 474-483

Shankar S (2016) Ecuador earthquake: death toll soars, aftershocks reported. International Business Times – 18 April

Sharma RD, Gupta S and Kumar S (1999) Application of extreme-value distribution for estimating earthquake magnitude-frequency relationships. Journal of Earthquake Technology 388(36): 15-26

Vanmarcke E, Heredia-Zavoni E and Fenton G (1993) Conditional simulation of spatially correlated ground motion. Journal of Engineering Mechanics 119(11): 2333-2352

Wiemer S (2000) Earthquake Statistics and Earthquake Prediction Research. Institute of Geophysics, Zürich, Switzerland. http://www.physics.buffalo.edu/phy410-505/midterm/img/wiemer-earthquake-prediction.pdf - [Accessed on 29.04.17]

## List of Tables



Table 1. Earthquake record database

| # | Earthquake(s) | Magnitude | Epicentral Distance Km | $vs_{30}$ ms$^{-1}$ | PGA g |
|---|---|---|---|---|---|
| 1-2 | Helena Montana-01, 10/31/1935, Carroll College, 180 / 270 | 6 | 2.86 / 2.92 | 593.35/551.82 | 0.16 |
| 3-4 | Northwest Calif-01, 9/12/1938, Ferndale City Hall, 45 / 224 | 5.5 / 5.8 | 53.88 / 53.77 | 219.31 | 0.15 / 0.11 |
| 5-6 | Izmir Turkey, 12/16/1977, Izmir, L / T | 5.3 | 3.21 | 535.24 | 0.42 / 0.13 |
| 7-8 | Dursunbey Turkey, 7/18/1979, Dursunbey, L / T | 5.34 | 9.15 | 585.04 | 0.18 / 0.24 |
| 9-10 | Imperial Valley-02, 5/19/1940, El Centro Array #9, 180 / 270 | 6.95 | 6.09 | 213.44 | 0.25 / 0.15 |
| 11-12 | Northern Calif-01, 10/3/1941, Ferndale City Hall, 225 / 315 | 6.4 | 44.68 | 219.31 | 0.10 / 0.12 |
| 13-14 | Northern Calif-03, 12/21/1954, Ferndale City Hall, 44 / 314 | 6.5 | 27.02 | 219.31 | 0.16 |
| 15 | Borrego Mtn, 4/9/1968, El Centro Array #9, 180 | 6.63 | 45.66 | 213.44 | 0.13 |
| 16-17 | San Fernando, 2/9/1971, Castaic - Old Ridge Route, 21 / 291 | 6.61 | 22.63 | 450.28 | 0.32 / 0.28 |
| 18-19 | San Fernando, 2/9/1971, LA - Hollywood Stor FF, 90 / 180 | 6.61 | 22.77 | 316.46 | 0.22 / 0.16 |
| 20 | San Fernando, 2/9/1971, Lake Hughes #1, 21 | 6.61 | 27.4 | 425.34 | 0.15 |
| 21-22 | San Fernando, 2/9/1971, Lake Hughes #12, 21 / 291 | 6.61 | 19.3 | 602.1 | 0.38 / 0.28 |
| 23-24 | Imperial Valley-06, 10/15/1979, Bonds Corner, 140 / 230 | 6.53 | 2.66 | 223.03 | 0.52 / 0.77 |
| 25-26 | Imperial Valley-06, 10/15/1979, El Centro Array #4, 140 | 6.53 | 7.05 | 208.91 | 0.48 / 0.27 |
| 27-28 | Imperial Valley-06, 10/15/1979, El Centro Array #5, 140 / 230 | 6.53 | 3.95 | 205.63 | 0.33 / 0.38 |
| 29-30 | Imperial Valley-06, 10/15/1979, El Centro Array #7, 140 / 230 | 6.53 | 0.56 | 210.51 | 0.34 / 0.47 |
| 31-32 | Kern County, 7/21/1952, Taft Lincoln School, 21 / 111 | 7.36 | 38.89 | 385.43 | 0.14 / 0.15 |
| 33-34 | Taiwan SMART1(45), 11/14/1986, SMART1 C00, EW / NS | 7.3 | 56.01 | 309.41 | 0.12 / 0.15 |
| 35-36 | Taiwan SMART1(45), 11/14/1986, SMART1 O02, EW / NS | 7.3 | 57.13 | 285.09 | 0.16 / 0.24 |
| 37-38 | Cape Mendocino, 4/25/1992, Petrolia, 0 / 90 | 7.01 | 8.18 | 422.17 | 0.58 / 0.66 |
| 39-40 | Landers, 6/28/1992, Lucerne, 260 / 345 | 7.28 | 2.19 | 1369 | 0.65 / 0.61 |

Table 2. Theoretical and simulated mean velocity $\overline{U}$ (ms$^{-1}$) and turbulence intensities

| Stats \ z (m) | 10 | 40 | 75 | 100 | 140 | 170 | 200 | 210 | 220 | 240 | 250 |
|---|---|---|---|---|---|---|---|---|---|---|---|
| $\overline{U}_t$ | 20.00 | 30.21 | 36.21 | 39.79 | 42.95 | 45.39 | 47.77 | 48.52 | 49.15 | 50.18 | 50.87 |
| $\overline{U}_s$ | 19.86 | 29.88 | 35.14 | 38.62 | 41.69 | 44.05 | 46.32 | 47.07 | 47.69 | 48.69 | 49.35 |
| $I_{u,t}$ | 0.295 | 0.206 | 0.244 | 0.221 | 0.195 | 0.172 | 0.146 | 0.137 | 0.130 | 0.116 | 0.107 |
| $I_{u,s}$ | 0.295 | 0.206 | 0.173 | 0.153 | 0.135 | 0.122 | 0.108 | 0.104 | 0.100 | 0.093 | 0.088 |

Table 3. Cross correlation results amongst the points of interest

| | 1 | 2 | 3 | 4 | 5 | 6 | 7 | 8 | 9 | 10 | 11 |
|---|---|---|---|---|---|---|---|---|---|---|---|
| 1 | **1.0000** | 0.4737 | 0.4100 | 0.2255 | 0.2134 | -0.0052 | -0.0591 | -0.1249 | -0.1843 | -0.1688 | -0.0237 |
| 2 | 0.4237 | **1.0000** | 0.6224 | 0.3814 | 0.2928 | 0.1594 | 0.0892 | 0.0231 | -0.0493 | -0.0151 | 0.0716 |
| 3 | 0.2090 | 0.4767 | **1.0000** | 0.6510 | 0.5322 | 0.2694 | 0.2860 | 0.2238 | 0.1078 | 0.1387 | 0.2322 |
| 4 | 0.1176 | 0.2605 | 0.5419 | **1.0000** | 0.7333 | 0.4118 | 0.4189 | 0.3157 | 0.2204 | 0.2723 | 0.2803 |
| 5 | 0.0653 | 0.1408 | 0.2895 | 0.5322 | **1.0000** | 0.6122 | 0.5377 | 0.4465 | 0.3681 | 0.3842 | 0.3309 |
| 6 | 0.0394 | 0.0831 | 0.1690 | 0.3092 | 0.5798 | **1.0000** | 0.5934 | 0.5431 | 0.5346 | 0.4584 | 0.3253 |
| 7 | 0.0231 | 0.0479 | 0.0961 | 0.1748 | 0.3265 | 0.5625 | **1.0000** | 0.8046 | 0.7388 | 0.6270 | 0.5227 |
| 8 | 0.0192 | 0.0394 | 0.0788 | 0.1429 | 0.2665 | 0.4588 | 0.8155 | **1.0000** | 0.8113 | 0.6355 | 0.5248 |
| 9 | 0.0164 | 0.0336 | 0.0669 | 0.1210 | 0.2255 | 0.3879 | 0.6893 | 0.8453 | **1.0000** | 0.7276 | 0.5858 |
| 10 | 0.0127 | 0.0257 | 0.0508 | 0.0917 | 0.1705 | 0.2929 | 0.5200 | 0.6376 | 0.7543 | **1.0000** | 0.7524 |
| 11 | 0.0106 | 0.0213 | 0.0420 | 0.0756 | 0.1403 | 0.2408 | 0.4274 | 0.5240 | 0.6198 | 0.8217 | **1.0000** |

Table 4. Geometry and natural frequency of wind turbines

| ID # | Height (m) | $D_{base}$ (m) | $D_{top}$ (m) | $t_{base}$ (m) | $t_{top}$ (m) | $n_0$ (Hz) |
|---|---|---|---|---|---|---|
| 1 | 150 | 7.5 | 4.0 | 0.05 | 0.016 | 0.44 |
| 2 | 200 | 10 | 7.5 | 0.075 | 0.018 | 0.34 |
| 3 | 250 | 15 | 10 | 0.10 | 0.025 | 0.24 |

Table 5. Total generalized forces $(F_{EQ}^* + F_W^*)$ acting on wind turbine towers (kN)

| $\bar{U}$ | H = 150 m | | | H = 200 m | | | H = 250 m | | | Average $F_{EQ}^* / F_W^*$ | | |
|---|---|---|---|---|---|---|---|---|---|---|---|---|
| ms$^{-1}$ | mean | rms | peak | mean | rms | peak | mean | rms | peak | mean | rms | peak |
| zero | 0.11 | 9.78 | 92.5 | 0.29 | 30.8 | 284 | 0.78 | 70.8 | 652 | - | - | - |
| 0.5 | 0.39 | 9.79 | 92.6 | 0.95 | 26.3 | 249 | 1.82 | 60.2 | 572 | 10.8 | 167 | 193 |
| 2.5 | 9.08 | 9.97 | 96.1 | 22.1 | 26.7 | 256 | 41.8 | 60.9 | 584 | 0.43 | 6.68 | 7.72 |
| 5 | 36.3 | 12 | 118 | 88.3 | 30.9 | 304 | 167 | 66.9 | 667 | 0.11 | 1.67 | 1.93 |
| 10 | 145 | 28 | 234 | 353 | 64.9 | 570 | 667 | 120 | 1137 | 0.03 | 0.42 | 0.48 |
| 15 | 326 | 58 | 471 | 794 | 133 | 1139 | 1500 | 235 | 2150 | 0.01 | 0.19 | 0.21 |
| 20 | 580 | 101 | 822 | 1411 | 232 | 1987 | 2666 | 405 | 3712 | 0.01 | 0.10 | 0.12 |

Table 6. Dynamic response amplitudes (m) calculated for wind turbine towers subject to $F_{EQ}^* + F_W^*$

| $\bar{U}$ | H = 150 m | | | H = 200 m | | | H = 250 m | | |
|---|---|---|---|---|---|---|---|---|---|
| ms$^{-1}$ | mean | rms | peak | mean | rms | peak | mean | rms | peak |
| zero | $9.3 \times 10^{-6}$ | 0.003 | 0.014 | $2.5 \times 10^{-5}$ | 0.005 | 0.017 | $2.6 \times 10^{-5}$ | 0.006 | 0.021 |
| 0.5 | $1.4 \times 10^{-4}$ | 0.003 | 0.015 | $2.2 \times 10^{-4}$ | 0.005 | 0.022 | $3.6 \times 10^{-4}$ | 0.007 | 0.026 |
| 2.5 | 0.003 | 0.004 | 0.017 | 0.005 | 0.006 | 0.023 | 0.009 | 0.009 | 0.029 |
| 5 | 0.013 | 0.006 | 0.030 | 0.021 | 0.009 | 0.046 | 0.034 | 0.015 | 0.067 |
| 10 | 0.051 | 0.016 | 0.090 | 0.083 | 0.030 | 0.155 | 0.137 | 0.046 | 0.229 |
| 15 | 0.116 | 0.035 | 0.197 | 0.187 | 0.067 | 0.342 | 0.309 | 0.101 | 0.507 |
| 20 | 0.205 | 0.061 | 0.349 | 0.333 | 0.119 | 0.605 | 0.549 | 0.179 | 0.898 |

Table 7. Probabilities associated to earthquake and wind events, and earthquake magnitudes across countries

| | *Probability of Exceedance, Seismic Magnitude per Country, or Wind Velocity* | | | | | | | | *a* | *b* |
|---|---|---|---|---|---|---|---|---|---|---|
| $P_W$ | 0.02 | 0.05 | 0.1 | 0.25 | 0.5 | 0.75 | 0.9 | 1 | - | - |
| $C_{prob}$ | 1 | 0.95 | 0.90 | 0.84 | 0.78 | 0.75 | 0.68 | 0.52 | - | - |
| $\bar{U}$ (ms$^{-1}$) | 20 | 18.92 | 18.05 | 16.75 | 15.53 | 14.49 | 13.68 | 10.33 | - | - |
| $P_{EQ}$ | 1 | 0.4 | 0.2 | 0.08 | 0.04 | 0.027 | 0.022 | 0.02 | - | - |
| India[1] | 3.19 | 3.67 | 4.04 | 4.52 | 4.88 | 5.09 | 5.19 | 5.24 | 4.35 | 0.83 |
| UK[2] | 2.06 | 2.44 | 2.74 | 3.12 | 3.42 | 3.59 | 3.66 | 3.71 | 3.82 | 1.03 |
| Turkey[3] | 1.96 | 2.48 | 2.87 | 3.39 | 3.78 | 4.01 | 4.11 | 4.17 | 3.21 | 0.77 |
| Greece[4] | 4.86 | 5.13 | 5.33 | 5.59 | 5.79 | 5.91 | 5.96 | 6.00 | 8.99 | 1.5 |
| Switzerland[5] | 3.54 | 3.96 | 4.27 | 4.68 | 5.00 | 5.18 | 5.26 | 5.31 | 5.1 | 0.96 |
| Global Data[1] | 6.36 | 6.73 | 7.02 | 7.39 | 7.68 | 7.84 | 7.92 | 7.96 | 8.44 | 1.06 |

[1] Sharma et al. (1999); [2] NERC (2017); [3] Bayrak et al. (2008); [4] Papazachos et al. (1997); [5] Wiemer (2000)

Table 8. Strength demands derived from the combined action of earthquake and wind

| Load Scenario | | Wind Speed $\bar{U}$ in ms$^{-1}$ | | | | | | | | |
|---|---|---|---|---|---|---|---|---|---|---|
| | | 0.00 | 10.33 | 13.68 | 14.49 | 15.53 | 16.75 | 18.05 | 18.92 | 20.00 |
| $I_{EQ+W}/I_{EQ}$ | EQ#1-40 | 1.0 | 9.36 | 16.13 | 18.07 | 20.73 | 24.11 | 27.98 | 30.76 | 34.43 |
| $I_{EQ+W}/I_W$ | EQ#1-40 | - | 0.305 | 0.525 | 0.588 | 0.674 | 0.784 | 0.910 | 1.00 | 1.12 |
| | EQ#5 $M_s$ = 5.3 | - | 0.314 | 0.541 | 0.606 | 0.696 | 0.809 | 0.939 | 1.032 | 1.157 |
| | EQ#24 $M_s$ = 6.53 | - | 0.367 | 0.632 | 0.708 | 0.813 | 0.945 | 1.097 | 1.206 | - |
| | EQ#38 $M_s$ = 7.01 | - | 0.346 | 0.596 | 0.668 | 0.766 | 0.890 | 1.033 | - | - |

Table 9. Strength and ductility demands derived from the combined action of earthquake and wind

| | Wind Speed $\bar{U}$ in ms$^{-1}$ | | | | | | |
|---|---|---|---|---|---|---|---|
| | 18.05 | | 18.92 | | | 20.00 | |
| Earthquake Event | EQ#24 | EQ#38 | EQ#1-40 | EQ#5 | EQ#24 | EQ#1-40 | EQ#5 |
| Strength Demand $I_{EQ+W}/I_{EQ}$ | 1.097 | 1.033 | 1.00 | 1.032 | 1.206 | 1.12 | 1.157 |
| Ductility Demand $\mu = u_{max}/u_y$ | 1.27 | 1.09 | 1.00 | 1.09 | 1.62 | 1.37 | 1.49 |

**List of Figures**



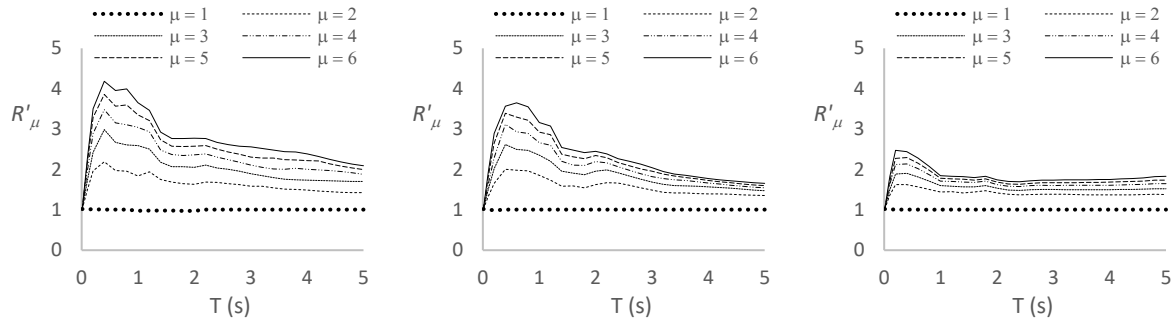


(a) $\Gamma = 60.43, \overline{U} = 15\ ms^{-1}$ (b) $\Gamma = 17.78, \overline{U} = 15\ ms^{-1}$ (c) $\Gamma = 1.91, \overline{U} = 15\ ms^{-1}$

Fig. 1. Strength reduction factors estimated for when $\overline{U} = 15\ ms^{-1}$
(Adapted from Martinez-Vazquez, 2017)

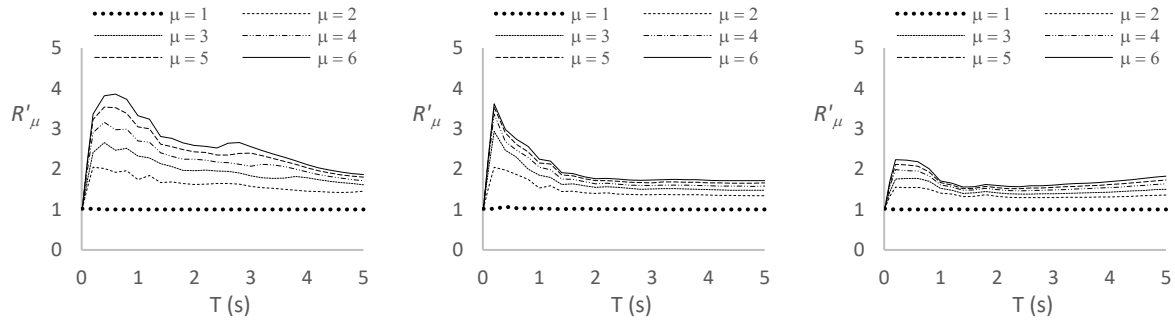


(a) $\Gamma = 60.43, \overline{U} = 20\ ms^{-1}$ (b) $\Gamma = 17.78, \overline{U} = 20\ ms^{-1}$ (c) $\Gamma = 1.91, \overline{U} = 20\ ms^{-1}$

Fig. 2. Strength reduction factors estimated for when $\overline{U} = 20\ ms^{-1}$
(Adapted from Martinez-Vazquez, 2017)